

GAP CLEARING KICKER MAGNET FOR MAIN INJECTOR

C. C. Jensen, R. Reilly, I. Terechkine, Fermilab*, Batavia IL 60510 U.S.A.

Abstract

A new fast extraction kicker magnet is required to clear the injection gap in the Main Injector at FNAL. An overview of the design choices is presented and the results of testing of the first prototype are discussed.

INTRODUCTION

These kicker system requirements were originally conceived for the NOvA project, a neutrino experiment located in Minnesota. To achieve the desired neutrino flux, several upgrades are required to the Main Injector (MI) accelerator and Recycler storage ring (RR) at Fermilab. One of these changes is a new gap clearing kicker in RR to reduce activation from beam loss. This new kicker will be used to extract uncaptured beam, created during the slip stack injection process [1], down the existing abort line. The MI would benefit from this gap clearing system immediately. A decision was made that early installation would be done in MI before moving the system to RR during NOvA. An identical system will be built for injection into the RR. Table 1 summarizes requirements for the kickers.

Table 1: Kicker System Requirements

	MI Gap Clearing	RR Gap Clearing	RR Injection
Angle	1.70 mrad	1.18 mrad	1.21 mrad
Field Rise	57 ns	57 ns	57 ns
Field Fall	400 ns	57 ns	57 ns
Pulse Width	1534 ns at 15 Hz burst rate		
Duty Factor	12 pulses per 1.33 seconds		
Stability	±3% of Nom. Flattop plus Pulse to Pulse		
Stability	±3% of Nom. Max. to Circulating Beam		

SYSTEM DESIGN

The MI gap clearing kicker system inherits features of previous fast kicker magnets [2, 3]. A thyatron switch will be used with coaxial cable pulse forming line (PFL). The cable will be pulse charged so that the thyatron can be run at high reservoir, and therefore high speed. The magnet will have a ceramic chamber with the required beam aperture. To fit the vacuum chamber, the magnetic aperture must be 53 mm x 110 mm. It will be a traveling wave magnet, e.g. a highly segmented LC network, so the pulse will propagate with limited distortion.

The load, matched to the cable impedance, will be mounted to the end of the magnet. Because a variety of

repetition rates are expected, the effect of average power on the magnet termination resistance has to be limited to ~1%. This has been done successfully on previous systems [4].

Given a previously demonstrated pulser voltage rise time (3% to 97%) of ~25 ns, the magnet fill time must be less than 32 ns to meet the field rise time requirement. As we rely on 50 Ω cable, the choices for the kicker impedance Z_0 are 50 Ω, 50/2 Ω, 50/3 Ω, etc. Vacuum and HV connections add ~0.5 m to the magnet length. Using 25 Ω or lower impedance would result in a lower ratio of the kicker magnetic length to its physical length. With the required aperture, rise time and 50 Ω impedance, the magnetic length is ~0.7 m. A maximum operating voltage of 55 kV on the thyatron then determines the maximum kick of 275 μrad per magnet.

While the rise and fall time for MI use are comparable to a previous kicker [2], meeting the fall time will be a new issue for the RR kickers. These kickers need a “bumper” system to cancel the tail and allow the system to meet the fall time requirement to the 3% level. This kicker system will consist of a pulsed power supply driving an additional kicker magnet mounted upside down and backwards in the tunnel. This requires complete mechanical symmetry in the magnet and is the final constraint on the magnet design.

MAGNET SIMULATION

Circuit Simulation

The first step in detailed design is a circuit simulation of the proposed magnet. It is known that parasitic elements in the magnet unit cell limit the bandwidth [5]. SPICE version 3F5 was used to simulate the magnet. The values for parasitic elements of the circuit, mainly capacitor inductance and cell-to-cell coupling, were taken from previous similar designs. These parameters depend strongly on the cell geometry and ferrite stacking factor. The stacking factor, the ratio of ferrite length to cell length, is a series of tradeoffs between high voltage hold off of the capacitor bus, field uniformity, required capacitance and manufacturing capability. This simulation showed that the rise time could be achieved with less than 30 cells, each 2.3 cm long. The final design has 27 ferrites and a stacking factor of 72%, which does not change the integrated field substantially and maintains adequate high voltage clearance and low inductance for the capacitor bus. Figure 1 shows schematic layout of one cell of the kicker. The ceramic vacuum chamber is located between the poles of ferrite flux return. The magnetic field is created by current in the high voltage and low voltage buses and the distance between the buses is adjustable.

* Fermilab is operated by Fermi Research Alliance, LLC. under Contract No. DE-AC02-07CH11359 with the US Department of Energy

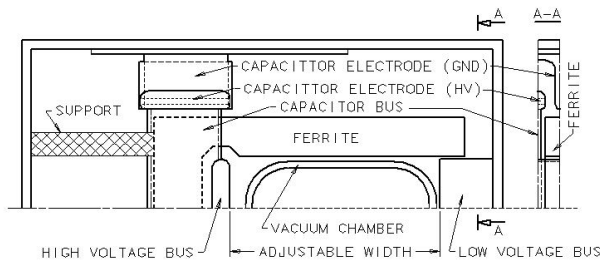


Figure 1: Cross-section of the kicker magnet; one quarter of one cell is shown.

The kicker design has to ensure a special value of the end capacitance. SPICE simulations of the magnet clearly showed a decrease in the field rise time when the end capacitance was between 50 and 60 pF. This value depends on input and output inductance and impedance match, but much larger or smaller capacitance values increase 3%–97% field rise time.

Field Simulation

Capacitor design was the most technically challenging part of the magnet. The capacitor had to have a tight tolerance on value, a long life and a low series inductance. The tight tolerance on the capacitance value required more than tight mechanical tolerances ($\pm 80 \mu\text{m}$). A 3D simulation of a cell of the magnet was ultimately done using COMSOL [6]. Approximately 15% of the capacitance is not from the HV capacitor electrode. Confidence in the modeling results was obtained by comparing the model with measurements on the prototype. The electrode design was for a peak electric field of not more than 9 kV/mm at a nominal voltage of 26 kV. A previous magnet [2] was designed, 2D, for a peak field of 8 kV/mm at 25 kV, and there have been no failures in $7 \cdot 10^8$ pulses at that voltage. The new limit is about 30% of the material breakdown, which under ASTM test method D149 is $\sim 21 \text{ kV}_{\text{rms}}/\text{mm}$. An operating level of 30% to 50% of breakdown is preferred to allow for surface imperfections. The parasitic capacitor inductance was kept low by making the capacitor bus (see Fig. 1) wide enough between the ferrites so it extended past the edge of the flux return.

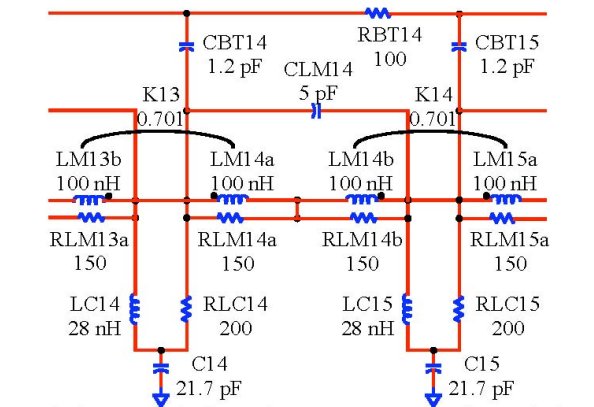
The ferrite cell was also simulated using COMSOL. One concern was high frequency dimensional resonance inside the ferrite itself. This resonance can appear in high permeability material with large sections. A study showed that with μ of 1500 and ϵ of 15, resonances can occur in the 40-50 MHz range. While permeability falls at these frequencies, a lower permeability material ($\mu = 400$) was chosen to lessen this effect. The smallest ferrite cross-section without significant saturation was also chosen.

One must also be able to adjust the average impedance of the magnet due to normal variations in capacitance and inductance. This adjustment is accomplished by trimming the low voltage bus in Fig. 1, which changes the inductance. This trimming is limited to about $\pm 5\%$ in inductance so it is also important to get the capacitance and inductance as close as possible to nominal values.

PROTOTYPING

The prototype magnet was built for several purposes: to determine the best ferrite material, to validate the field modeling, to validate the circuit modeling and to perform high voltage life testing. The ferrite material chosen was based on performance in the prototype magnet. Testing of three materials, with μ of 300, 400 and 550 showed that magnet cells made with μ of 400 had the lowest overshoot at the output. We believe this is mainly due to higher ferrite losses.

The circuit model shown in Fig. 2 was based on measurements from the prototype magnet. This model is significantly different from the original design model in that the stray inductance (LC) is much less, the coupling (K) between cells is higher and of the opposite polarity, and the equivalent ferrite loss (RLM) is much higher. While the values of LC, LM, K, C, CBT and RBT in Fig. 2 are based on measurements, RLM and RLC are chosen for a best fit of simulation to the measurements. These parameters are frequency dependant, but this feature was not included in the model. Since lossy dispersion was not done correctly, there is a poor match of the output voltage rise time between modeled (29 ns) and measured (37 ns).



LM inductance in ferrite, main gap, no current in adjacent ferrite
 RLM loss in ferrite, main gap
 LC inductance in capacitor bus, between ferrites
 RLC loss in ferrite, capacitor bus
 K coupling between adjacent ferrites, SPICE definition
 C main capacitor
 CBT capacitance from HV bus to coating inside vacuum chamber
 RBT resistance of coating inside vacuum chamber
 CLM capacitance between adjacent capacitor buses

Figure 2: Equivalent circuit: two mid-magnet cells.

Validation of the electric field simulations of the cell capacitance was most critical. A model of a bare HV bus cell was compared to measurements of the bare HV bus with ends. Careful measurements of the capacitance at the ends of the magnet were also made. The total measured capacitance was 6 pF larger than the total of prediction from model plus end measurements. This difference was attributed to the end but was not verified by modeling to find a source of the discrepancy. The model prediction for the prototype configuration was 21.5 pF per cell with

potting ϵ of 2.74 and ferrite ϵ of 14. The measurement gave a value of 21.9 pF, including the end correction above, with estimated potting ϵ of 2.74. One possible source for this difference is the procedure to extract the cell capacitance from the measured total magnet capacitance. Another source can be the dielectric properties of the ferrite material, which contribute about 9% to the total cell capacitance, but are not well controlled.

The dielectric constant for the potting material, Sylgard 184, was also determined from measured capacitance before and after potting. The data sheet ϵ is 2.75 when cured at 65 C for 4 hours. Initially, ϵ was 2.79 and came down to 2.73 after 4 months, but it was cured at room temperature. This is done to prevent the potting from pulling away from the materials with different expansion coefficients as the magnet cools. This separation could cause air gaps to form and compromise the insulation.

High voltage testing of the prototype was done for about 4 months at the nominal repetition rate. The magnet was driven at 26 kV for $2 \cdot 10^7$ pulses and at 30 kV for 10^7 pulses without any failures. Because this is only 1% of the desired lifetime, 60 Hz corona testing of the prototype and first production magnet are to take place shortly.

Following the high voltage pulse testing of the magnet, final changes were made to the drawings and almost all parts for the eight production magnets were ordered. The final magnet cross sections are shown in Fig 3.

While measurements showed fairly good agreement with the model, it is still possible to get outside the desired capacitance range; therefore capacitors for only the first three magnets were ordered so that production could start.

Pulse testing of the first production magnet has just recently begun. The inductance, capacitance and complex impedance were measured with an AC impedance bridge. A procedure for adjusting the magnet impedance by trimming the low voltage bus was carried out which achieved 50Ω at $1 V_{rms}$. The magnet was then moved to a high voltage testing area with an existing pulser. Measuring the reflection from the high power load at 6 kV, the impedance is about 52Ω and at 24 kV, the impedance is about 53Ω . The impedance match should be closer, but the capacitance between HV bus and beam tube was much lower than in the prototype. A slight mismatch between load and magnet (with the load being 2% smaller) reduces the field rise time. However, there was a substantial undershoot ($\sim 10\%$) on magnet input voltage due to excessive capacitance at the load. The capacitance of the load was much larger than estimated. The SPICE model was then modified to match the measurement and the effective capacitance of the load was determined. The input (and output) capacitance will now be changed for the remaining magnets to produce the desired response, shown in Fig. 3. Further details on simulations and measurements are included in the design report [7].

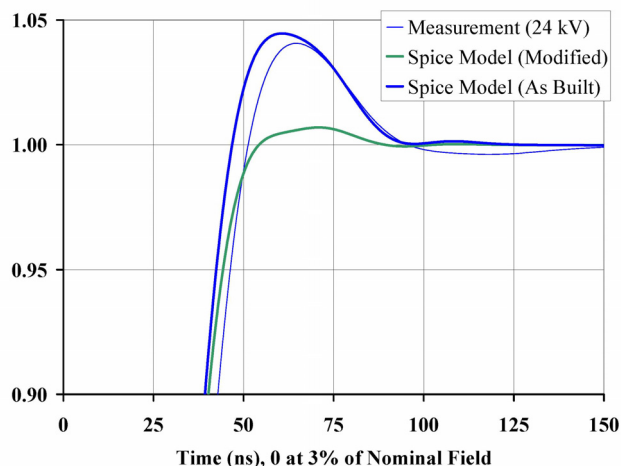


Figure 3: Calculated and measured integrated magnetic field; model with reduced capacitance.

CONCLUSIONS

The magnet parameters and performance of the system has been compared to the models. We expect that the performance specifications will be met with the slight end modification and production will continue. Seven magnets are scheduled to be installed summer of 2009 in MI and six more magnets, including the bumper, are scheduled for installation in the RR in early 2012.

This magnet collaboration was across two divisions and four groups at Fermilab. Thanks to all who contributed thoughts and effort.

REFERENCES

- [1] K. Seiya, "Progress in Multi-Batch Slip Stacking in the Fermilab Main Injector and Future Plans", PAC2009
- [2] D. Qunell, C. Jensen, D. Tinsley, "Kicker System for 8 GeV Proton Injection", PAC1997, pp1287-1289
- [3] C. Jensen, B. Hannah, R. Reilly, "A Fast Injection Kicker for the Tevatron", PAC2001, pp3720-3723
- [4] S. Reeves, C. Jensen, "Numi Proton Kicker Extraction Magnet Termination Resistor System", PAC2005, pp2224-2226
- [5] G. Nassibian, "Traveling Wave Kicker Magnets with Sharp Rise and Less Overshoot", IEEE Trans. Nucl. Sci., Vol 26, pp.4018-4020, 1979
- [6] COMSOL, Vers. 3.4, Multiphysics with AC/DC Module, COMSOL Inc, Burlington MA 01803
- [7] C. Jensen, MI Gap Clearing Kicker Magnet Design Review, Fermilab TM-2429-AD